Effects of Cloud Horizontal Inhomogeneity on the Optical Thickness Retrieved from Moderate-Resolution Satellite Data

HIRONOBU IWABUCHI AND TADAHIRO HAYASAKA

Center for Atmospheric and Oceanic Studies, Tohoku University, Sendai, Miyagi, Japan

(Manuscript received 13 June 2001, in final form 9 November 2001)

ABSTRACT

Cloud remote sensing techniques are conventionally based on the independent pixel approximation (IPA). Here, three-dimensional (3D) radiative effects on IPA-based retrieved optical thickness from a visible-wavelength moderate-resolution (about 1 km) sensor are investigated. A Monte Carlo 3D radiative transfer model and a lognormal spectral cloud model are used to simulate monochromatic radiance reflected from overcast boundary layer cloud. A characterization of statistical properties of the optical thickness by the mean (M) and variance (S^2) of the logarithm of the optical thickness is proposed, where S represents a degree of cloud inhomogeneity. Biases in retrieved values of the two parameters with the IPA are defined as ΔM and ΔS^2 and attributed to neglect of net horizontal radiative transport in the IPA. Sensitivities of ΔM and ΔS^2 are tested with respect to geometrical roughness, M, S, mean geometrical thickness, spectral exponent of optical thickness fluctuation, ground surface reflectance, and bidirectional angles. The 3D radiative effects are sensitive to the geometrical roughness of cloud top rather than internal inhomogeneity of the extinction coefficient. The bias ΔM is negative in forward scattering viewing geometry due to cloud-side shadowing, while positive in backscattering viewing geometry due to side illumination. It is found that ΔM is proportional to S^2 and large for a dense cloud. On the other hand, ΔS^2 largely depends on the solar zenith angle; smoothing is exhibited for high solar elevation and roughening for low solar elevation. The smoothing and roughening phenomena are found to be almost independent of the inhomogeneity parameter. An optically thick cloud exhibits more roughening, while for a geometrically thick cloud both smoothing and roughening are enhanced. It is suggested that for the bias removal some empirical assumptions are required in geometrical and microphysical properties of cloud, which should be studied with in situ observation data.

1. Introduction

Clouds exhibit horizontal and vertical inhomogeneity though they have been assumed to be plane-parallel and homogeneous (PPH) in all applications of the one-dimensional radiative transfer theory (e.g., climate simulation and remote sensing). The deviation of actual cloud from PPH cloud model produces two problems. One is a direct problem, that is, how we calculate the radiometric quantities, such as flux and radiance when an inhomogeneous cloud field is given a priori. We need both an exact solution and approximate methods with less computational effort. The other is the inverse problem, that is, remotely sensed cloud properties are biased due to 3D radiative effects. A correction to conventional method or new retrieval method is required.

Related to the direct problem, many theoretical studies have pointed out that the domain-averaged reflectance of inhomogeneous cloud field is different from the PPH one (e.g., Barker and Davies 1992a; Kobayashi 1993; Cahalan et al. 1994b; Loeb et al. 1998; Várnai 2000). Cahalan et al. (1994a) have demonstrated that the mesoscale-averaged albedo is approximated with the independent pixel approximation (IPA), which uses 1D radiative transfer theory at local scale with net horizontal transport of radiation ignored. The IPA provides good accuracy for the domain-averaged flux at spatial scale larger than about 3 km, in the case of boundary layer cloud field (Duda et al. 1996; Barker 1996). It should be noted that the IPA is applicable to neither radiance nor local pixel radiometric quantity (Marshak et al. 1995a,b; Loeb et al. 1998; Zuidema and Evans 1998; Várnai 2000). The 3D radiance is affected by many factors. Kobayashi (1993) has demonstrated that cloud inhomogeneity effects on domain-averaged radiance for bumpy cloud-top model depends on the bidirectional viewing geometry and the mean optical thickness. Loeb et al. (1998) and Várnai (2000) suggested that variation of cloud-top height affects the reflection more than that of internal volume extinction does. The cloud inhomogeneity also affects the spatial variability of radiometric quantity as well as domain average (Marshak et al. 1995a,b; Zuidema and Evans

Corresponding author address: Dr. H. Iwabuchi, Hydrological Cycle Research Program, Frontier Research System for Global Change, 3173-25 Showa-machi, Kanazawa-ku, Yokohama, Kanagawa 236-0001, Japan.
E-mail: hiro-iwabuchi@jamstec.go.jp

1998; Várnai 2000; Oreopoulos et al. 2000). The deviation of 3D exact solution from the IPA is explained by effects of net horizontal radiative transport (Várnai and Davies 1999; Marshak et al. 1999). For instance, so-called ''smoothing'' and ''roughening'' are explained by net horizontal radiative transport (Marshak et al. 1995a,b; Oreopoulos et al. 2000). The smoothing is explained by diffusion of photons in a multiple scattering process. When the solar elevation is low, the roughening comes from enhanced spatial variability of direct and low-order scattering solar radiations incident to horizontally inhomogeneous cloud columns.

On the inverse problem, a limited number of methods for correction of retrieved cloud parameter are presented. In optical remote sensing of cloud parameters, such as cloud optical thickness and effective particle radius, the retrieval for a pixel is performed by comparison between observed reflectance and results of 1D radiative transfer calculation for PPH cloud model (e.g., Nakajima and King 1990). The IPA is implicitly employed in that procedure. The earlier works suggested that the retrieved parameter would be considerably biased by the neglect of cloud horizontal inhomogeneity. Barker and Liu (1995) have presented a correction of the domain average of retrieved optical thickness with respect to the geometrical thickness of flat cloud. Chambers et al. (1997) have investigated effects of geometrical aspect ratio on the domain average of retrieved optical thickness and proposed a correction method, with the assumption of flattop and bumpy bases of cloud. Although these two studies are based on a flattop cloud model, it has been suggested that reflection from bumpy-top cloud is largely different from flattop cloud (Loeb et al. 1998; Várnai and Davies 1999).

In these situations, the 3D radiative effects on local-scale reflected radiance are not sufficiently clear. This problem is closely associated with the inverse problem. The important factors are at least degree of cloud inhomogeneity, mean optical thickness, cloud geometry (e.g., thickness, aspect ratio, and cloud-top bumpiness), the bidirectional angles (solar and viewing angles), and also spatial resolution. For domain-averaged optical thickness, the 3D radiative effects have been parameterized with a single parameter in a few studies (e.g., Barker and Liu 1995; Chambers et al. 1997). At least, two parameters are necessary to correct retrieved optical thickness, since not only average but also variance of reflectance is affected by the 3D radiative effects (Marshak et al. 1995a,b; Várnai 2000). The objectives of the present study are to investigate properties of solar reflected radiation from inhomogeneous cloud at visible wavelength and to evaluate the 3D effects on cloud optical thickness retrieval from visible-wavelength moderate-spatial-resolution data (about 1 km). For such moderate resolution, we can never obtain the information about inhomogeneity in a pixel, though this information is necessary to interpret the reflectance of the pixel. For this reason, we take a statistical approach in which the statistical quantities of retrieved cloud optical thickness in the $(8\ \text{km})^2$ domain are used to describe the 3D radiative effects. Sensitivities of the 3D radiative effects are tested with respect to some cloud geometrical and microphysical parameters. This paper is organized in the following way. Section 2 describes the Monte Carlo radiative transfer model and stochastic cloud models. In section 3, a characterization of cloud inhomogeneity effects is presented. In section 4, sensitivities of the 3D radiative effects to some parameters are tested. In section 5, applications to bias removal will be discussed. Finally, section 6 describes a summary and concluding remarks.

2. Models

a. Monte Carlo radiative transfer model

A radiative transfer model employed here uses a forward Monte Carlo photon tracing technique. The Monte Carlo technique is time-consuming but we can obtain the exact solution to 3D radiative transfer. A three-dimensional Monte Carlo radiative transfer model was developed based on Hayasaka et al. (1995). In our model, a trajectory of photon is traced until the photon exits from top or bottom of model atmosphere. All photons exiting from the bottom are reflected back to model atmosphere by the underlying surface, which is assumed to be Lambertian. The maximum number of surface reflection events is limited to two, and all photons going incident to the surface in three times are assumed completely absorbed by the surface. Avoiding too many reflections between cloud and surface, this procedure saves computation time with sufficient accuracy when the surface reflectance (α_g) is less than about 0.2. After tracing the trajectory, a probability of absorption by gases, cloud droplets, and surface is calculated from a pathlength and the number of scattering events in each layer and the surface. The gaseous absorption coefficients are provided from the Low-resolution Transmission-7 (LOWTRAN-7) database (Kneizys et al. 1988).

Figure 1 shows a vertical cross section of the model atmosphere. The atmospheric compositions such as the water vapor and the ozone are given from U.S. standard atmosphere (Kneizys et al. 1988). The model atmosphere is divided into four layers, including cloud in the second layer from the bottom. The cloud layer is horizontally divided into 256^2 grid boxes [the entire domain is $(8\ \text{km})^2$ and a grid spacing is 31.25 m], while the other layers are assumed homogeneous. The cloud inhomogeneity is given down to the spatial scale of 31.25 m. A cyclic boundary condition is assumed. In general, computation time for Monte Carlo simulation increases with increasing number of grids in model atmosphere. In our model, vertical grids in the cloud layer are not divided discretely. Heights of cloud top and base are arbitrarily given for each horizontal grid box. The computation time is thus saved even if geometrically rough

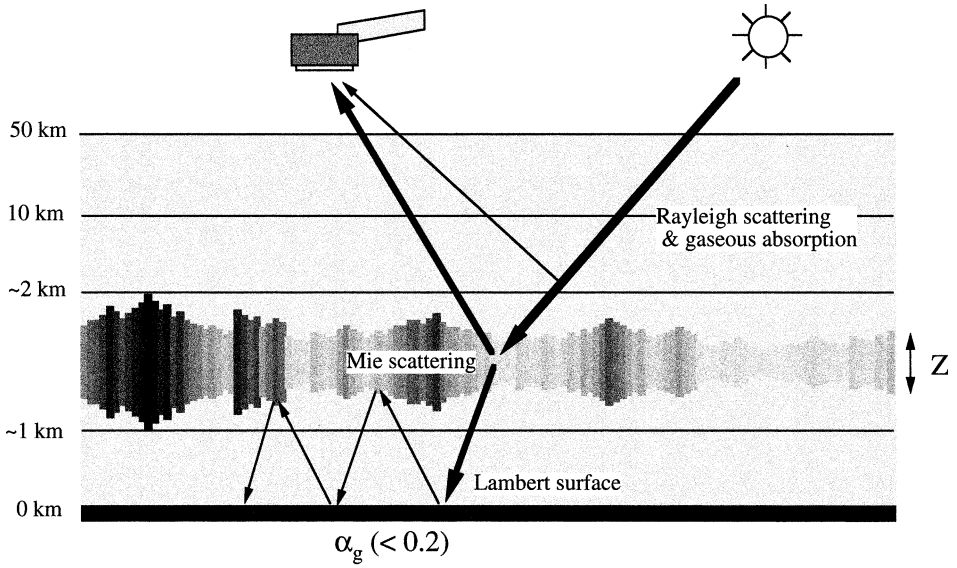

FIG. 1. Vertical cross section of atmospheric model used in Monte Carlo radiative transfer. In the cloud layer, the entire domain [(8 km)^2] is divided into 256^2 grids, and cloud inhomogeneity is given down to the spatial scale of 31.25 m. Heights of cloud top and base are arbitrarily given for each cloud column in a horizontal grid box. The other layers are assumed horizontally homogeneous.

cloud field is given. The cloud droplets are assumed to be water phase and to have a lognormal size distribution with an effective particle radius of 10 μm and a standard deviation of ln(1.3). The single scattering properties of cloud droplets were calculated by Mie theory at a wavelength of 0.64 μm, which is the center of Advanced Very High Resolution Radiometer (AVHRR) channel 1. The single scattering albedo is 0.999997 at this wavelength; the scattering is almost conservative.

The radiance field is calculated for each pixel with the spatial resolution of 1 km (i.e., 8^2 pixels in the domain). For each pixel, the bidirectional reflection function (BRF; R) is defined as

$$R(x, y, \mu_0, \mu, \phi) = \frac{\pi I(x, y, \mu_0, \mu, \phi)}{\mu_0 F_0}, \qquad (1)$$

where I is the radiance (W m^{-2} sr^{-1} μm^{-1}); F_0 is the solar irradiance (W m^{-2} μm^{-1}) at the top of atmosphere; x and y are horizontal coordinates; μ_0 and μ are cosines of the solar and viewing zenith angles, respectively; and ϕ is relative azimuth angle of outgoing ray from incoming ray ($\phi = 0°$ corresponds to forward scattering viewing geometry). The azimuth of initial incident direction is fixed to the negative direction along the x axis. The bin intervals for μ and ϕ are 0.1 and 30°, respectively. In the present study, each simulation used 10^7 photons. Monte Carlo noise gives rise to uncertainty in the calculated BRF. The root-mean-square errors of a pixel BRF and domain average are estimated at about 2% and 0.25%, respectively, where the accuracy was checked by comparisons with the discrete ordinate method for plane-parallel cloud models. The accuracy is sufficient to investigate statistical properties, such as mean and variance.

b. Cloud model

A spectral model as in Evans (1993) was used in the present study to generate artificial cloud realization. Stochastic models have been developed to simulate the fractal properties, such as the bounded cascade (Cahalan et al. 1994b) and the spectral models (Barker and Davies 1992a; Evans 1993; Titov 1998). A common property among them is that the power spectrum of the cloud optical thickness (or the liquid water content) is scale-invariant and obeys to the power law (i.e., $P \sim k^{-\beta}$, where k denotes the wavenumber, and β the spectral exponent). The power-law behavior has been often observed for stratocumulus cloud (e.g., Barker and Davies 1992b; Davis et al. 1997), and the spectral exponent has been close to 5/3 corresponding to the Kolmogorov–Obukhov law. In the present study, it is assumed that the frequency distribution of the optical thickness is lognormal. The distribution function [$p(\tau)$] is written in the following form:

$$p(\tau) = \frac{1}{\sqrt{2\pi}s} \exp\left[-\frac{(\ln\tau - m)^2}{2s^2}\right], \qquad (2)$$

where m and s^2 denote mean and variance of lnτ, respectively. It has been reported that the frequency distribution of optical thickness has a positive skewness rather than having a Gaussian distribution (Hayasaka et al. 1994; Cahalan et al. 1994b; Oreopoulos and Davies 1998b). The large positive skewness is important for

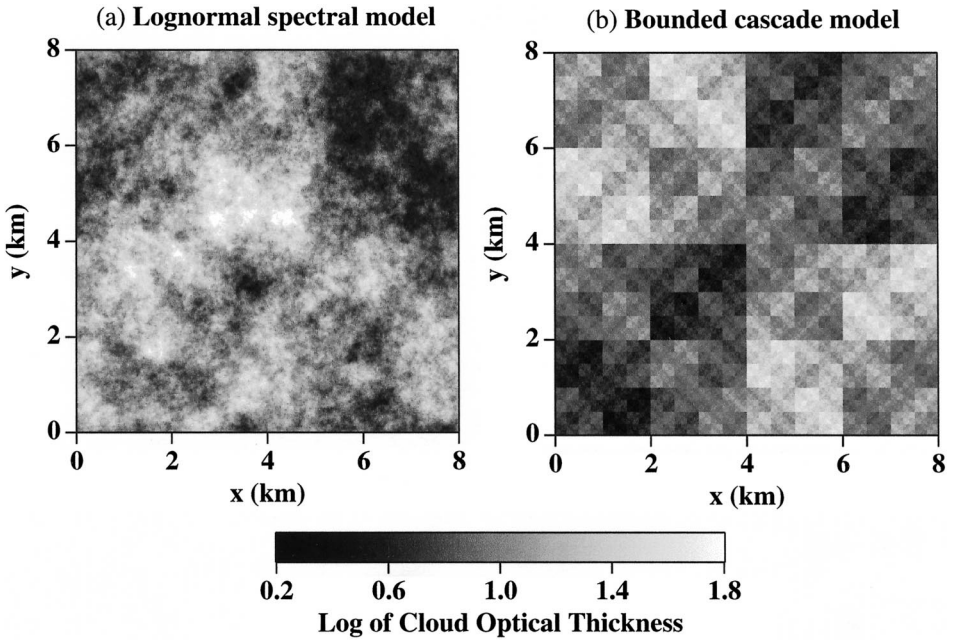

FIG. 2. Images of base 10 logarithm of the optical thickness artificially generated by (a) lognormal spectral model and (b) bounded cascade model. These images are generated with common parameters; $M = 1$, $S = 0.3$, $\beta = 1.6$ (M and S are mean and standard deviation of $\log\tau$, and β is the spectral exponent). The corresponding parameters for the bounded model are set as $f \approx 0.41$ and $H \approx 0.5$ (Cahalan et al. 1994b; Marshak et al. 1995b). The domain size is $(8\ \text{km})^2$ and a pixel size is $(31.25\ \text{m})^2$.

realistic radiative properties of inhomogeneous cloud (Cahalan et al. 1994b).

First, in the practical procedure, Gaussian noise with amplitude of unity and random phase is generated in Fourier space. Second, the amplitude is scaled by $k^{-\beta/2}$ (k is the wavenumber). The inverse Fourier transformation makes an isotropic, scale-invariant, Gaussian field. Next, skewness and kurtosis are checked, and the case with a large deviation of skewness from zero, or kurtosis from three, is excluded and a calculation restarts from the first step. Next, the linear conversion is operated in order that the Gaussian field possesses arbitrarily given mean and variance (m and s^2, respectively). Finally, the exponential conversion completes a lognormal spectral model. The exponential conversion little alters the power-law scaling property of the optical thickness fluctuation. The two-dimensional version of this model was used. Figure 2a shows an example of the optical thickness image generated by the lognormal model. It is known that no orientation is present; the fluctuation is isotropic.

The bounded cascade model has been often used to study the radiative effects of cloud inhomogeneity (Cahalan et al. 1994a,b; Marshak et al. 1995a,b; Oreopoulos et al. 2000; Szczap et al. 2000). The bounded cascade model is compared with the lognormal spectral model (section 4b). A two-dimensional bounded cascade uses checkerboard-like pattern in each cascade process, and this is a simple extension of the one-dimensional bounded cascade in Cahalan et al. (1994b). An example is shown in Fig. 2b. This model also has the characteristics of the power-law spectrum and the lognormal frequency distribution and requires the same three parameters (m, s^2, and β) as the lognormal model. Differences between the two models are that the bounded cascade model has $\beta = 1$–2 while β is arbitrary in the spectral model, and the bounded one has discontinuity (localized inhomogeneity) in optical thickness fluctuation.

In order to examine effects of geometrical roughness on radiative properties, four models were considered (Fig. 3): FC (flat cloud) and RC1 to RC3 (rough cloud) models. The FC model exhibits flat top and flat bottom. For the RC models, either bottom (RC1) or top (RC3) is rough, or both are rough (RC2). It is noted that the domain-averaged geometrical thickness and the local optical thickness of each cloud column are the same among the four models and that vertical homogeneity is assumed. For the RC models, the local geometrical thickness (Z,) in each column is associated with the local optical thickness (τ) through

$$\frac{Z}{\sqrt{\tau}} = \frac{\langle Z \rangle}{\langle \sqrt{\tau} \rangle}, \tag{3}$$

where the operator $\langle \cdot \rangle$ denotes domain average (also hereafter). A similar relationship has been reported observationally in Minnis et al. (1992). The variation of the optical thickness comes from the variation of extinction coefficient solely in the FC model, while it comes additionally from the geometrical thickness in

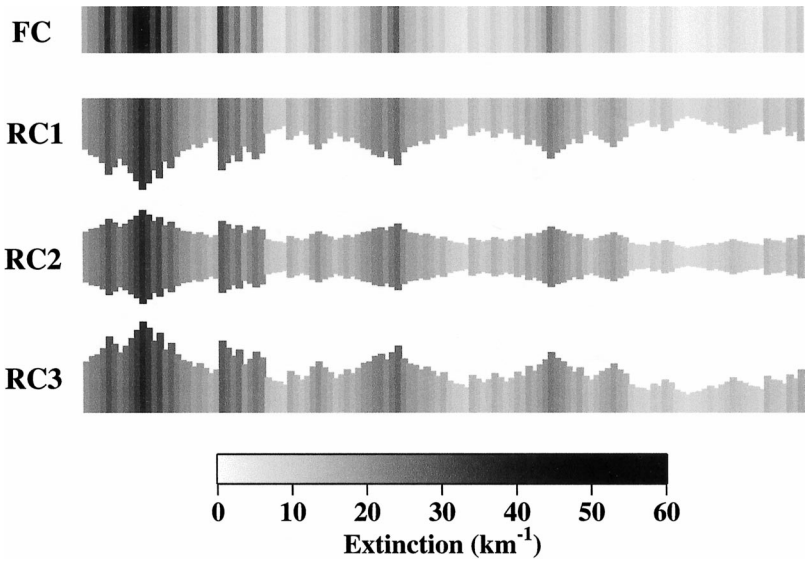

FIG. 3. Vertical cross sections of four cloud models used to examine effects of geometrical roughness on reflection properties of cloud. The FC model has flat top and flat bottom. For the RC models, either bottom (RC1) or top (RC3) is rough, or both (RC2) are rough. The domain-averaged geometrical thickness and the local optical thickness of each column are the same among the four models.

the RC models. The FC model thus possesses larger variability of in-cloud extinction coefficient than the RC models.

3. Representation of horizontal inhomogeneity effects

In this section, cloud inhomogeneity effects on the frequency distribution of retrieved optical thickness are introduced. Figure 4 shows theoretical relationships of BRF with $\log\tau$ for PPH cloud model (here and hereafter, the base of logarithm is 10). It is well known that the BRF is approximately linear to $\log\tau$ for moderate τ. The linearity is marked for $\log\tau = 0.5$–1.5 ($\tau \approx 3$–30). When

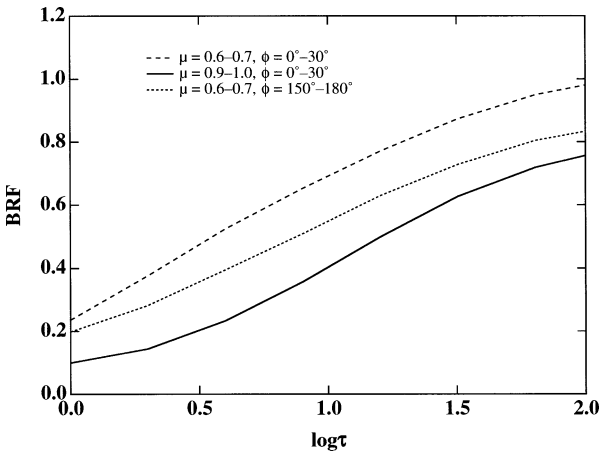

FIG. 4. Theoretical relationships of BRF with base 10 $\log\tau$ for plane-parallel and homogeneous cloud model; $\mu_0 = 0.5$.

the net horizontal radiative transport is absent, that is, when the IPA works perfectly, moments of BRF are closely associated with moments of $\log\tau$ rather than moments of τ. We shall consider the first and the second moments. Here, M and S^2 are defined as mean and variance, respectively, of the logarithm of the optical thickness. The IPA-assumed BRF (R_{ipa}) is almost equal to the BRF for plane-parallel cloud with $\log\tau = M$; that is, $R_{\text{ipa}} \approx R_{\text{pph}}(\log\tau = M)$. This concept is equivalent to the effective thickness approximation in Cahalan et al. (1994b), who have applied it to calculation of the domain-averaged albedo. More precisely, R_{ipa} is approximated by the averaged BRF with weighting by assumed analytic function for frequency distribution of optical thickness. When the frequency of optical thickness obeys lognormal distribution, R_{ipa} is calculated from two parameters, M and S (i.e., lognormal IPA as in Oreopoulos and Davies 1998b).

The first and second moments of optical thickness are determined from M and S in analytic form when the frequency distribution of optical thickness is lognormal. The mean optical thickness $\langle\tau\rangle$ follows:

$$\log\langle\tau\rangle = M + \frac{\ln 10}{2}S^2. \tag{4}$$

According to satellite cloud climatology, global mean optical thickness is about 9 for all clouds and 6–8 for low clouds (Rossow and Schiffer 1991; Kawamoto et al. 2001). The ''reduction factor'' ($\chi \equiv 10^{-\Delta}$, where $\Delta \equiv \log\langle\tau\rangle - M = \ln 10/2 \cdot S^2$) in Cahalan et al. (1994b) decreases with increasing S. The parameter S roughly determines the difference between the plane-parallel ap-

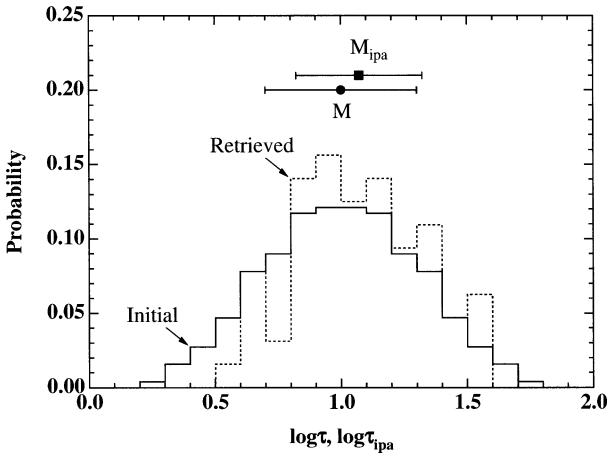

FIG. 5. An example of frequency distributions of true (initial) optical thickness (τ) and retrieved one (τ_{ipa}) for inhomogeneous cloud field. Marks in the upper part denote mean values of logτ (circle) and logτ_{ipa} (square), and bars corresponding standard deviation. The mean and variance of logτ are defined as M and S, respectively, and M_{ipa} and S_{ipa} are also defined similarly. The optical thickness was retrieved from BRF of $\theta_0 = 60°$, $\mu = 0.7$–0.8, $\phi = 150°$–$180°$ for a single RC2 realization with $S = 0.3$, $M = 1$, $\langle Z\rangle = 500$ m, $\beta = 1.6$, and $\alpha_g = 0.06$.

proximation [$R_{pph}(\log\tau = \log\langle\tau\rangle)$] and the effective thickness approximation [$R_{pph}(\log\tau = M)$]. An inhomogeneity parameter (ρ_τ) in Davis et al. (1997) and Szczap et al. (2000) is expressed with S in the following form:

$$\rho_\tau \equiv \frac{\sigma_\tau}{\langle\tau\rangle} = \sqrt{\exp[(S\ \ln 10)^2] - 1}, \tag{5}$$

where σ_τ denotes the standard deviation of the optical thickness. Thus, ρ_τ has one-to-one relation with S when the frequency distribution of optical thickness is lognormal. The parameter S is a measure of degree of cloud inhomogeneity. According to Zuidema and Evans (1998), $S = 0.1$–0.3 in 7-km domain for stratocumulus clouds during the Atlantic Stratocumulus Transition Experiment (ASTEX). Our 6-yr analyses of satellite data over the northeastern Asian seas also indicated a variety of the inhomogeneity parameter with respect to season and geographical region; $S = 0.03$–0.3 in (9 km)^2 domain for overcast boundary layer clouds (Iwabuchi 2000).

Figure 5 shows an example of the frequency distribution of initial and retrieved optical thickness for cloud field with $S = 0.3$. Conventional IPA inversion was used to retrieve the optical thickness from BRF. Here, M_{ipa} and S^2_{ipa} are defined as mean and variance, respectively, of the logarithm of retrieved optical thickness. It is known from Fig. 5 that both M_{ipa} and S^2_{ipa} are biased. The biases, ΔM and ΔS^2, are defined as

$$\Delta M \equiv M_{ipa} - M, \tag{6a}$$

$$\Delta S^2 \equiv S^2_{ipa} - S^2. \tag{6b}$$

The bias ΔM implies a difference in average BRF between IPA and 3D radiative transfer. And ΔS^2 implies the spatial variability (smoothness/roughness) of BRF. It is noted that variability is masked out at smaller scale than the spatial resolution (1 km in this paper) of the simulated BRF and this masking effect is involved in ΔS^2.

When the BRF is larger than $R_{pph}(\tau = 128)$ or smaller than $R_{pph}(\tau = 1)$, it is difficult to retrieve optical thickness from reflection measurements because of low sensitivity of BRF to the optical thickness (Fig. 4). In the former case, retrieved optical thicknesses were all set at 128 in the present study. The latter situation frequently occurs in observation of broken cloud field. In such a case, M_{ipa} and S_{ipa} were estimated with the following method: a truncated normal distribution fitting (TNDF) method. In the TNDF method, it is regarded that pixels with $\tau > 1$ indicate cloudy sky and the rest is clear sky. After the M_{ipa} and S_{ipa} are initialized to values for cloudy pixels, the following processes are iterated.

- The frequency distribution of logτ for $\tau < 1$ is virtually assumed to be a truncated part of normal distribution with mean and standard deviation of M_{ipa} and S_{ipa}, respectively. The virtual part is weighted by clear-sky fraction.
- Two moments, M_{ipa} and S_{ipa}, are renewed from a combination of the frequency distribution for $\tau > 1$ and the virtual part for $\tau < 1$.

The above iteration is continued to obtain a unique set of M_{ipa} and S_{ipa}. The TNDF method works well except when cloudy-sky fraction is small (<0.5). It is possible to estimate M_{ipa} and S_{ipa} of rather broken cloud field by using this method.

4. The biases in retrieved optical thickness

In this section, sensitivities of ΔM and ΔS^2 are tested on cloud geometrical roughness, frequency distribution of optical thickness, and other parameters [spectral exponent (β), mean geometrical thickness ($\langle Z\rangle$), and ground surface reflectance (α_g)]. To test sensitivities, we refer to a standard case with $M = 1.0$, $S = 0.3$, $\beta = 1.6$, $\langle Z\rangle = 500$ m, and $\alpha_g = 0.06$. Corresponding mean and standard deviation of optical thickness is 12.7 and 9.7, respectively.

a. Effects of geometrical roughness

Figure 6 shows relationships of ΔM and ΔS^2 with the viewing angle, for the four cloud models (FC, RC1, RC2, and RC3, as in Fig. 3). The results are shown for near the solar plane; that is, $\phi = 0°$–$30°$ in the left-hand side of the figure and $\phi = 150°$–$180°$ in the right-hand side (hereafter ''forward view'' and ''backward view,'' respectively, at oblique sun). The bias ΔM has small negative value for overhead sun (the solar zenith angle

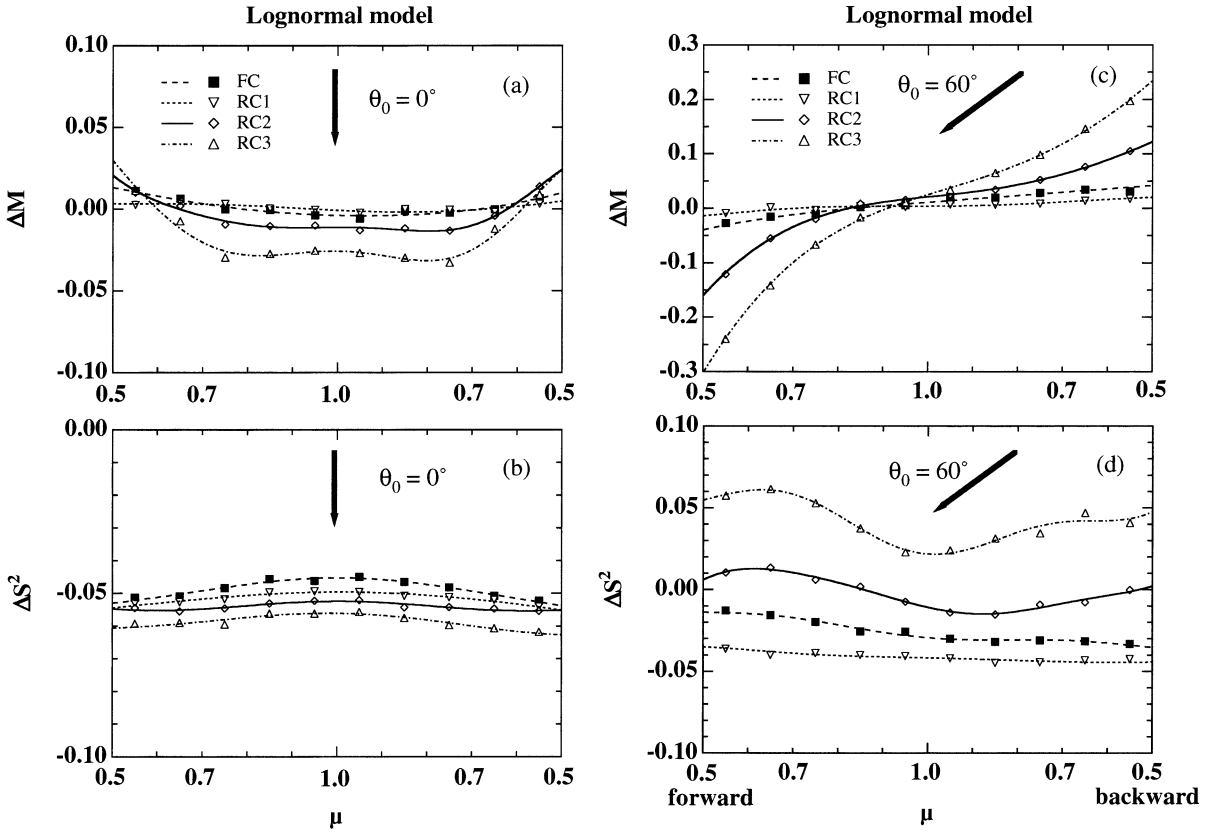

FIG. 6. Viewing angle distribution of the biases ΔM (a,c) and ΔS^2 (b,d) for the four cloud models; FC, RC1, RC2, RC3. The results were averaged over three cloud realizations generated by lognormal spectral model. The solar zenith angle (θ_0) is 0° (a),(b) or 60° (c),(d). The relative azimuth angle between solar and viewing directions is 0°–30° in the left-hand side of these figures and 150°–180° in the right-hand side.

$\theta_0 = 0°$). This is ascribed to tilted cloud surface, which reflects the photons in off-nadir direction and darken the near-nadir reflection. For oblique sun ($\theta_0 = 60°$), ΔM is negative in forward view due to cloud side shadowing, while positive in backward view due to cloud side illumination. Tendency of the cloud 3D effect is common among the four cloud models though its magnitude differs substantially and increases in the following order: RC1, FC, RC2, RC3. In addition to in-cloud variation of extinction coefficients, the variation of cloud-top height enhances 3D effects. For RC2, ΔM is -0.04 in the forward view and 0.07 in the backward view with $\mu = 0.7$. For RC3, ΔM is -0.12 and 0.14 in the two directions, respectively. It is suggested that the variation of cloud-top height is important for the bidirectional reflection, as suggested by Loeb et al. (1998) and Várnai and Davies (1999). The bumps at cloud top allow the horizontal transport of a large amount of the incident and reflected solar radiation. It is found from Fig. 6 that the 3D radiative effect for the FC model is larger than the RC1 model. The reason is attributable to large variability of the extinction coefficient near cloud top of FC rather than RC1. Most of photons are reflected from the upper part of cloud layer, so the inhomogeneity near cloud top is important. It is suggested that the optical thickness retrieval is not sufficiently accurate without information of cloud geometrical roughness, especially in off-nadir view with oblique sun. For this reason, it is recommended that optical thickness retrieval is restricted to close nadir-viewing geometry if conventional IPA is applied to oblique sun.

The 3D radiative effect on the spatial variability of reflected radiance significantly differs among the four models (Figs. 6b,d); large ΔS^2 indicates large spatial variability of reflected radiance. The value of ΔS^2 increases in the following order: RC3, RC2, RC1, FC for $\theta_0 = 0°$; RC1, FC, RC2, RC3 for $\theta_0 = 60°$. When the solar elevation is high, ΔS^2 takes a large negative value. This indicates that the spatial variability of reflected radiance is small due to the smoothing by photon diffusion in multiple scattering process (Marshak et al. 1995a; Davis et al. 1997). More smoothing effect is shown for the model with a bumpy cloud top that allows more horizontal radiative transport than a flat cloud top. When solar elevation is low, the opposite effect, roughening, is introduced by enhanced variability of direct and low-order scattering radiative incidence to inho-

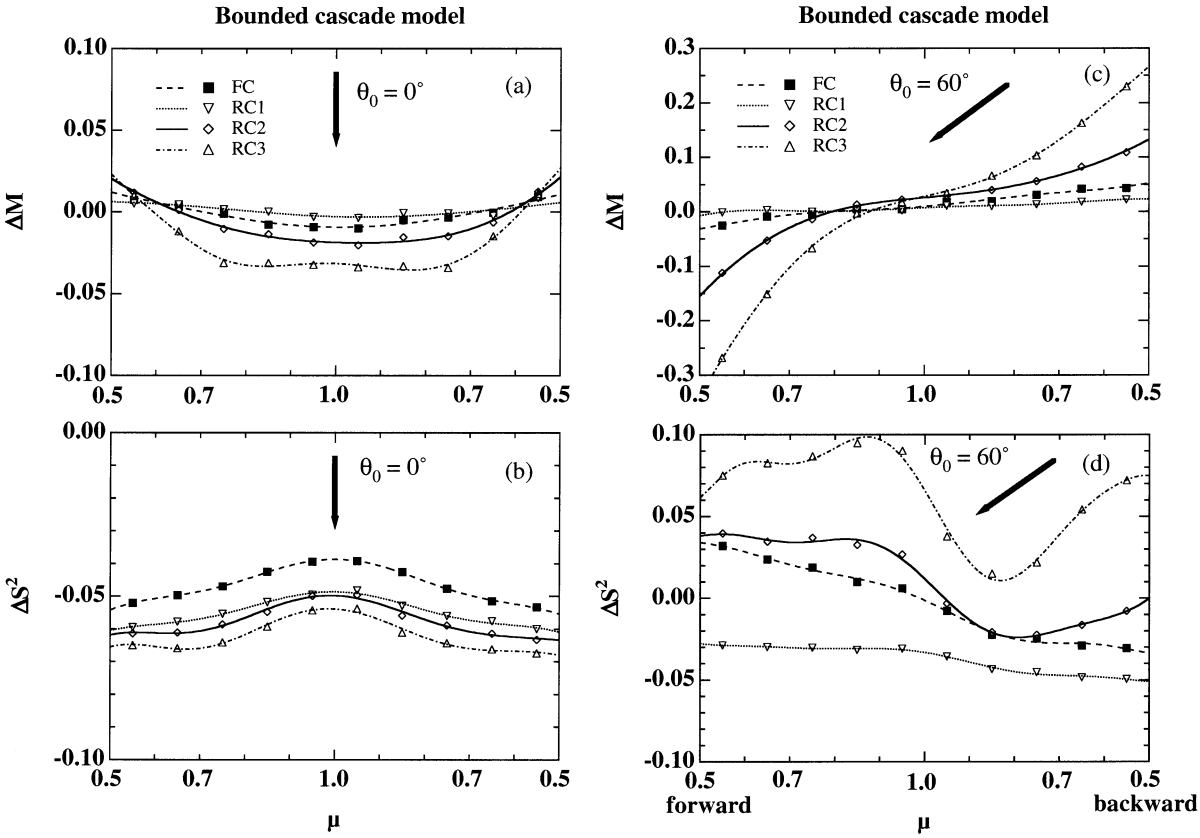

FIG. 7. As in Fig. 6, except for bounded cascade model.

mogeneous cloud column. It is found that the roughening effect is sharp for bumpy cloud top and closely associated with the cloud top structure. In Fig. 6d, there is a tendency for the roughening to be sharper in the forward view than in the backward view. This is because both bright and dark regions of cloud surface are viewed in that geometry; the former is illuminated by the direct solar beam and the latter is shadowed by optically dense part. On the other hand, bright parts are mainly viewed in the backward direction, with the contrast of brightness decreasing.

b. Lognormal model versus bounded cascade model

Figure 7 is the same as Fig. 6 except for the bounded cascade model. It is found that ΔM (Figs. 7a,c) is almost the same as for the lognormal spectral model, despite the apparent difference in their geometrical shapes as shown in Fig. 2. On the other hand, clear difference is shown for ΔS^2 (Figs. 7b,d). For geometrically rough cloud models (especially RC3), there is a tendency that ΔS^2 for the bounded model has a complicated angular distribution. At overhead sun, ΔS^2 for the bounded model has a large angular difference between nadir and off-nadir directions; while at oblique sun, a maximum is found in near-nadir forward view around $\mu = 0.85$ and a minimum in the backward view around $\mu = 0.85$. The discontinuities are present in the optical thickness fluctuation generated with the bounded cascade model, and that would be associated with the complicated angular dependence of ΔS^2. According to Davis et al. (1997), the ''fractionally integrated'' model (nearly the same as the lognormal spectral model in this paper) is good for simulating observed liquid water fluctuations. These results show that the bounded model is not appropriate for investigating bidirectional angular dependence of 3D radiative effects, especially for bumpy cloud. The discontinuities of the optical thickness are associated with vertical walls at the cloud surface for RC2 and RC3 models. It is suggested that the gradient of cloud surface affects the spatial distribution of reflectance dominantly.

c. Sensitivity tests

In this section, sensitivities of the 3D radiative effects to several parameters are tested. Here and hereafter, a bumpy-top, bumpy-base model (RC2) is used. Many observations of boundary layer cloud with lidar, radar, and stereo-photography have shown that top and bottom of cloud are rough (Boers et al. 1998; Kikuchi et al. 1993; Vali et al. 1998). From our analyses of satellite observation data, it has been shown that cloud-top bumps like RC2 are reasonable to explain the observed

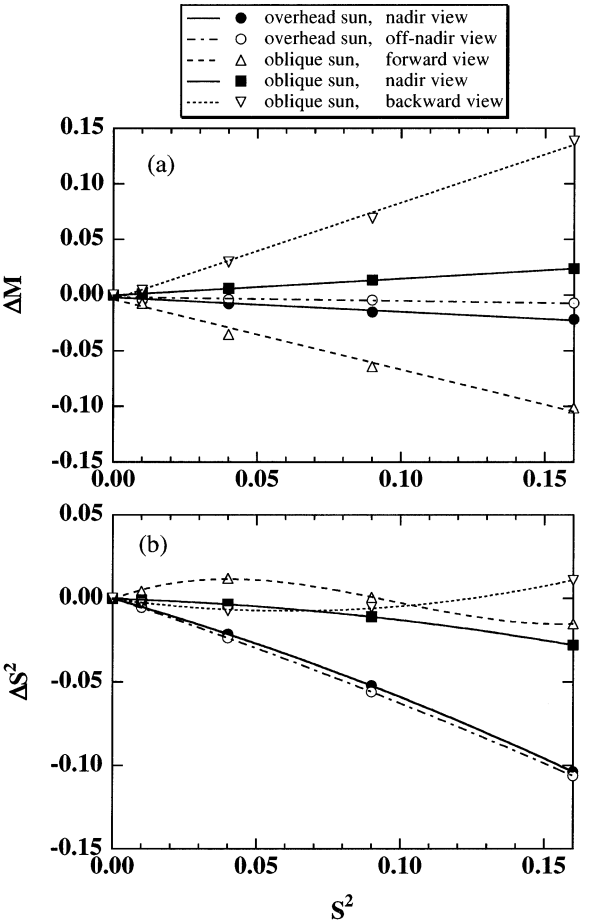

FIG. 8. IPA biases (a) ΔM and (b) ΔS^2 as a function of the inhomogeneity parameter S for overhead sun ($\theta_0 = 0°$) and oblique sun ($\theta_0 = 60°$). "Nadir view," $\mu = 0.9$–1.0, $\phi = 0°$–$30°$; "off-nadir view," $\mu = 0.6$–0.7, $\phi = 0°$–$30°$; "forward view," $\mu = 0.6$–0.7, $\phi = 0°$–$30°$; "backward view," $\mu = 0.6$–0.7, $\phi = 150°$–$180°$.

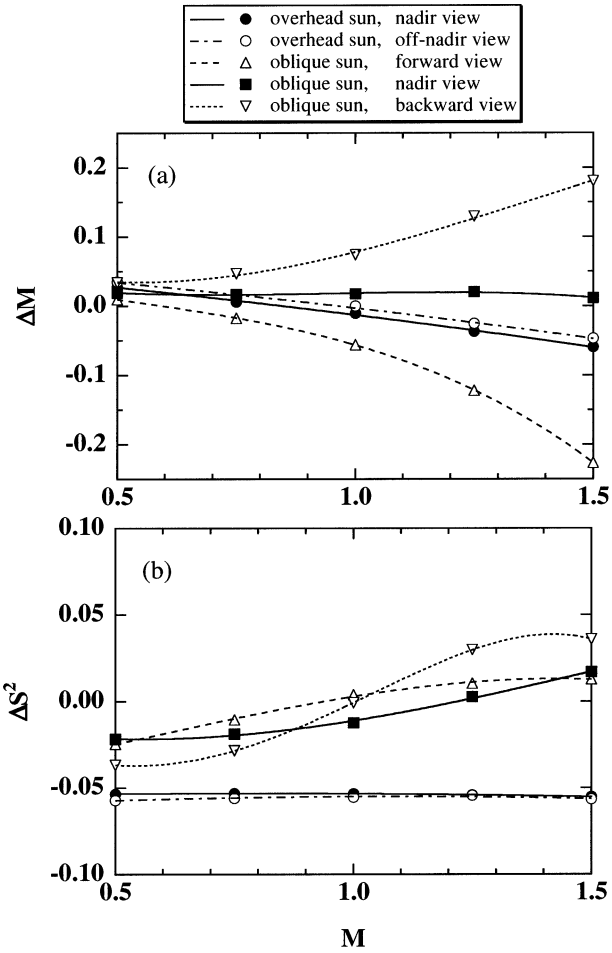

FIG. 9. As in Fig. 8, except for as a function of M.

angular dependence of retrieved optical thickness (Iwabuchi 2000).

Figure 8 shows sensitivities of ΔM and ΔS^2 to the inhomogeneity parameter S ($S = 0.0$–0.4). A large value of S is associated with large variability of cloud-top height, where the standard deviation of cloud-top height is 28, 55, 83, and 107 m for $S = 0.1$, 0.2, 0.3, and 0.4, respectively. It is found that ΔM is almost proportional to S^2 (Fig. 8a). The absolute value of ΔM increases with increasing S, so that the cloud 3D effects on brightness (e.g., brightening and darkening) are governed by the parameter S. It is found that the parameter S is important to describe the radiative effect of cloud inhomogeneity. On the other hand, ΔS^2 is roughly proportional to S^2, and the proportionality is good except for off-nadir view with oblique sun. In other words, relative bias $\Delta S^2/S^2$ is almost constant with respect to the bidirectional angle. This means that the smoothing and roughening phenomena are almost independent of the degree of horizontal inhomogeneity. Thus, the two-parameter representation (with M and S^2) simplifies the 3D radiative effect dependence on the degree of inhomogeneity. A little increase in ΔS^2 is shown in the backward view at large S^2 and this is regarded partly due to low sensitivity of BRF to $\log\tau$ for optically thick cloud (Fig. 4); the positive bias in mean brightness increases variability of inverted $\log\tau$ when cloud inhomogeneity is very large.

Figure 9 shows sensitivities of ΔM and ΔS^2 to M ($M = 0.5$–1.5). A high sensitivity of ΔM to M is found, especially for off-nadir view with oblique sun. The difference in ΔM between the forward and backward views increases for optically thick cloud field. The geometrical roughness for RC2 model is unchanged by M because it is determined by S uniquely, so that a change in M means a change in the cloud density. It is thus known that the 3D effects on brightness are sharp for optically thick cloud. In Fig. 9b, ΔS^2 increases with increasing M for oblique sun while almost independent of M for overhead sun. It is suggested that the roughening is sharp for optically thick cloud. This is because, for dense cloud, a photon travels a short distance horizontally from incident position at cloud surface and the reflected photon possesses localized information of cloud vari-

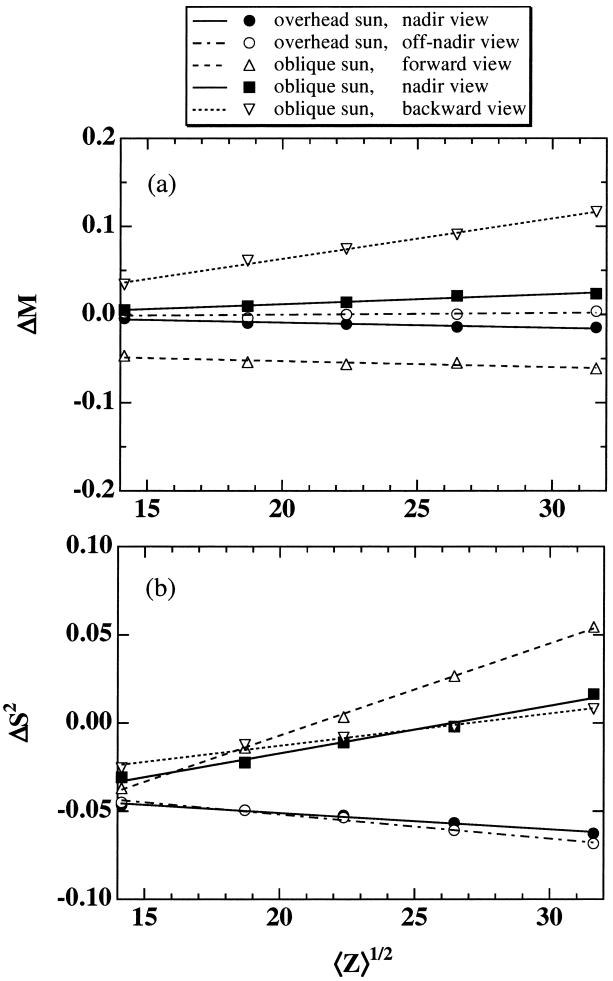

FIG. 10. As in Fig. 8, except for as a function of the mean geometrical thickness $\langle Z \rangle$.

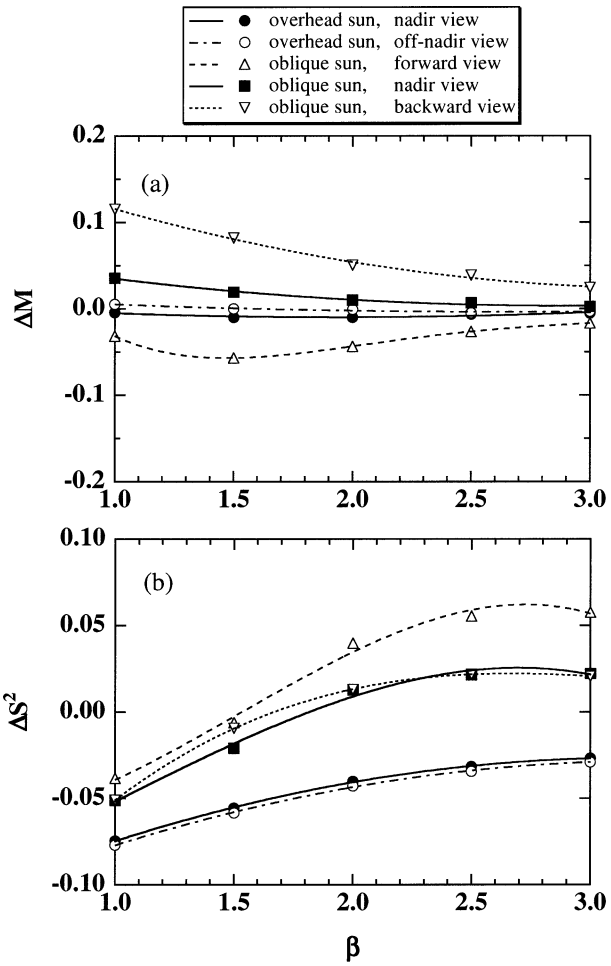

FIG. 11. As in Fig. 8, except for as a function of the spectral exponent β.

ability. The increase of ΔS^2 with increasing M is not sharp for $M > 1.2$ in the backward view. Since a retrieved value M_{ipa} is relatively very large when M is as large as 1.5, the retrieval of S^2_{ipa} for such optically thick cloud is affected by many pixels with larger BRF than $R_{\text{pph}}(\tau = 128)$, whose retrieved value is forced to be 128.

Figure 10 shows the sensitivity of ΔM and ΔS^2 to the mean geometrical thickness ($\langle Z \rangle = 200$–1000 m) with constant M and S. It is shown that ΔM and ΔS^2 are almost linear to the square root of $\langle Z \rangle$. The difference in ΔM between forward and backward views is large for geometrically thick cloud. However, ΔM does not change dramatically, in spite of the fivefold increase in $\langle Z \rangle$ (from 200 to 1000 m). It is found that relative importance of $\langle Z \rangle$ for the 3D effect is smaller than S and M as described above. The effect of $\langle Z \rangle$, however, may be more significant if $\langle Z \rangle$ increases simultaneously with M; for optically thick cloud, 3D effects will be more sensitive to geometrical thickness than for optically thin cloud. In Fig. 10b, the bias ΔS^2 increases with increasing $\langle Z \rangle$ at overhead sun, whereas it decreases at oblique sun. A wide cloud side allows greater transport of horizontal radiation, so both smoothing and roughening are enhanced.

Figure 11 shows sensitivities of ΔM and ΔS^2 to the exponent of power-law spectrum of optical thickness fluctuation ($\beta = 1$–3). A small value of β means that amplitude of optical thickness fluctuation is relatively large at small spatial scale; the fluctuation is close to white noise. In Fig. 11a, the tendency of ΔM for β is similar to what Barker and Davies (1992a) have shown for flux albedo. A main feature is that the deviation of 3D reflectance from the IPA (absolute value of ΔM) increases with decreasing spectral exponent. There is a tendency for ΔM to increase with decreasing β for $\beta < 1.5$; that is, the field becomes more reflective for white noise-like cloud. Even in the forward view ΔM increases with approach to white noise-like cloud. This is ascribed to the illumination effect by small cloud elements predominant over the shadowing effect, which works effectively only when horizontal optical thickness of the

TABLE 1. Primary and secondary factors related with 3D radiative effects.

Primary factor	Secondary factors
Geoetrical inhomogeneity	Morphology
	Inhomogeneity parameter (S)
	Geometrical thickness (Z)
Internal inhomogeneity	Inhomogeneity parameter (S)
	Mean optical thickness ($\langle\tau\rangle$ or M)
	Geometrical thickness (Z)
Horizontal scale	Spatial resolution
	Spectral exponent (β)
Angular geometry	Bidirectional angles (θ_0, θ, ϕ)

cloud element is large enough. On the other hand, ΔS^2 increases monotonically with β (Fig. 11b). The increase of ΔS^2 is because the variability is masked at smaller spatial scale than the spatial resolution of calculated radiance (1 km in the present study). The variance of $\log\tau$ at the spatial scale larger than 1 km increases with increasing β if the variance in the entire domain is constant.

It is important to test effects of the ground surface reflectance (α_g) on the horizontal radiative transport, since actual reflectance of the earth's surface largely varies in time and space. Respective relationships between BRF and $\log\tau$ for each α_g were calculated from 1D theory and used to retrieve optical thickness based on IPA. This procedure implies that cloud remote sensing is performed assuming ground surface reflectance determined previously, as in the procedure of the International Satellite Cloud Climatology Project (ISCCP; Rossow and Schiffer 1991), where monthly mean surface reflectance is prepared from observation of clear-sky pixels before cloud detection and optical thickness retrieval. It was found that ΔM and ΔS^2 are little sensitive to α_g (not shown) when the surface is not very reflective ($\alpha_g < 0.2$), except for desert and ice sheet. The result suggests that parameterizations for ΔM and ΔS^2 can be simplified for a variety of surface reflectance.

5. Discussion

In previous sections, it was quantitatively shown that the biases, ΔM and ΔS^2, are functions of M, S, mean geometrical thickness, spectral exponent, and surface reflectance. The biases correspond to changes in mean brightness and variance, respectively, as results of the 3D radiative effect. Table 1 summarizes the primary and secondary factors related with 3D radiative effects. All of them are important for interpreting the 3D radiative property, while in 1D radiative transfer, all of the required factors are bidirectional angles and optical thickness. To correct the 3D effect on retrieved optical thickness, some empirical assumptions will be required because some factors are difficult to estimate from optical remote sensing. It is useful to make some parameterizations available for interpretation of the multiple relationships on the above various parameters. Such efforts are described in the appendix. Using the parameterizations, we can remove the bias from statistical quantity of IPA-based retrieved optical thickness although assumptions are required for mean geometrical thickness and spectral exponent.

The angular dependence of the 3D effect suggests that satellite-derived optical thickness is systematically larger in the backward view than in the forward view. Loeb and Coakley (1998) have reported a systematic decrease of observed optical thickness with viewing angle in the forward view, and their results are consistent with the results presented here. Although a clear increase of observed optical thickness in the backward view was not reported in Loeb and Coakley (1998), a possible reason for the discrepancy may be ascribed to degradation in spatial resolution of AVHRR with increasing viewing zenith angle. For a wide field-of-view, frequent contamination of dark clear-sky to broken cloud pixel decreases observed optical thickness on average. As for variance, Oreopoulos and Davies (1998a) have reported the solar zenith angle dependence of variance of $\log\tau_{ipa}$, which was remotely sensed by using AVHRR data. In their results, the variance of $\log\tau_{ipa}$ systematically increases with an increase of solar zenith angle for $\theta_0 = 50°$–$80°$, and the tendency is consistent with the results presented here. For viewing angle dependence, Oreopoulos and Davies (1998a) have reported that the variance of $\log\tau_{ipa}$ increases substantially from the forward view to the backward view. However, the viewing angle dependence would be nominal since the viewing angle is well correlated with the solar zenith angle in their AVHRR observation (Fig. 2 in Oreopoulos and Davies 1998a). The variance of $\log\tau_{ipa}$ highly depends on the solar zenith angle rather than the viewing zenith angle. It is noted that in the present study, the pixel size is fixed, not depending on the viewing angle. In a real scanning radiometer, it is the angular step that is constant and the spatial resolution at the surface degrades with increasing viewing angle. A main result of the degradation would be a decrease in variance because of averaging in-pixel variation of reflectivity. Obviously, the mean brightness does not differ with the spatial resolution. In actual observations, spatial variability for off-nadir view would be smaller than examined here.

In practical procedure for optical remote sensing, the viewing angle is restricted less than about 45° (e.g., Kawamoto et al. 2001). If so, the viewing angle dependence of retrieved optical thickness is not very problematic. The solar zenith angle dependence, however, should be corrected since ΔS^2 highly depends on the solar zenith angle. For instance the logarithm of the mean retrieved optical thickness is roughly estimated as $\log\langle\tau_{ipa}\rangle \approx M_{ipa} + \ln 10/2\,(S_{ipa})^2$. For $\theta_0 = 0°$, 60°, 70°, $\log\langle\tau_{ipa}\rangle = 1.036, 1.109, 1.229$, respectively, in the nadir-viewing standard case of RC2 with $M = 1$, $S = 0.3$, $\langle Z\rangle = 500$ m, $\beta = 1.6$, and $\alpha_g = 0.06$. The corresponding values of mean retrieved optical thickness are 10.9,

12.9 and 16.9, respectively, while the true value is 12.7. This solar angle dependence of the mean retrieved optical thickness may appear in the cloud climatology. It has been reported in ISCCP product that annual zonal-mean optical thickness of low-clouds increases with increasing latitude from about 5 at the equator to about 12 at 60° north and south (Tselioudis et al. 1992; Drake 1993). The seasonal changes have also been shown. The latitudinal and seasonal changes might be partly affected by the cloud inhomogeneity. In addition, the observed inhomogeneity parameter would highly depend on the solar zenith angle, as suggested from AVHRR observations (Oreopoulos and Davies 1998a; Pincus et al. 1999). Global observation of the inhomogeneity parameter and correction of 3D radiative effects may bring on revised climatology of cloud optical thickness.

We have investigated the 3D radiative effects with some assumptions in cloud model; the cloud morphology, the relation of the geometrical thickness with the optical thickness [Eq. (3)], the vertical homogeneity of cloud microphysics, and the neglect of small-scale variability ($<$31.25 m). The cloud-top bumpiness has been reported for boundary layer clouds (Boers et al. 1988; Kikuchi et al. 1993), despite frequent uses of flat cloud model to study 3D radiative effects (e.g., Cahalan et al. 1994a; Marshak et al. 1995a,b; Szczap et al. 2000). As shown in section 4a, cloud-top bumpiness plays a dominant role in determining the 3D radiative effects. General properties of cloud-top bumps and its relation to cloud microphysics should be modeled using in situ observation data. Regarding the vertical inhomogeneity, it is well known that the cloud water is concentrated in the upper part of boundary layer cloud (Bower et al. 1994). The radiative effect of the concentration on cloud top would be nearly the same as for a dense cloud. The validity of the relation of $Z \sim \tau^{0.5}$ is unknown at present, especially at small spatial scale. The 3D effects would be enhanced if the geometrical thickness was more sensitive to the local optical thickness; for instance, $Z \sim \tau^{0.6}$ as an adiabatic parameterization in Pawlowska et al. (2000). In situ observations for various types of cloud are required for empirical parameterization. In addition, the neglect of small-scale variability may enhance the 3D effects. It must be clarified for practical application of correction to the retrieval.

6. Summary and conclusions

In the present study, we have investigated the 3D radiative effects on the statistical quantities of optical thickness of overcast boundary layer cloud retrieved with the independent pixel approximation (IPA) from visible-wavelength moderate-resolution data. A Monte Carlo radiative transfer model was used to compute radiance reflected from inhomogeneous cloud. We have proposed a characterization of inhomogeneous cloud by mean (M) and variance (S^2) of logarithm of the optical thickness, where S represents a degree of horizontal inhomogeneity. These statistical quantities dominantly determine the 3D radiative effects. The mean and variance of logarithm of IPA-based retrieved optical thickness are biased because the IPA neglects the effects of net horizontal radiative transport. These biases were defined as ΔM and ΔS^2 and investigated in detail. Conclusions from the present study are summarized as follows.

- The 3D radiative effects depend on M, S, the mean geometrical thickness, and the spectral exponent of optical thickness fluctuation. Domain-averaged radiative property is a function of not only the mean of cloud quantities, but also inhomogeneity of them. The inhomogeneity parameter S is important to represent a degree of horizontal inhomogeneity and its radiative effects. It is recommended that a parameter of this kind would be included to the compilation of satellite cloud climatology in the future.
- The 3D radiative effects highly depend on the geometrical roughness of cloud, especially of cloud top. Clouds with bumpy tops exhibit more 3D radiative effects (e.g., brightening, darkening, smoothing and roughening) than clouds with flat tops. No significant difference in ΔM appears between the lognormal spectral model and the bounded cascade model. On the other hand, ΔS^2 for the bounded cascade model has complicated angular dependence.
- Large bias ΔM is found in the off-nadir view with oblique sun. The darkening of mean reflectance is exhibited in forward scattering viewing geometry due to cloud-side shadowing, while brightening in backscattering viewing geometry due to cloud side illumination. It was found that ΔM is proportional to S^2 and large for a dense cloud. It is suggested that the viewing angle should be restricted to less than about 45° if conventional IPA is applied.
- The bias ΔS^2 largely depends on the solar zenith angle. The effects of radiative smoothing and roughening are dominant at overhead sun and oblique sun, respectively. The smoothing and roughening phenomena are found to be almost independent of the inhomogeneity parameter. An optically thick cloud exhibits more roughening, while for a geometrically thick cloud both smoothing and roughening are enhanced.
- The solar zenith angle dependence of these 3D radiative effects derives bias in mean retrieved optical thickness; retrieved optical thickness of inhomogeneous cloud with the IPA increases with increasing solar zenith angle when data in near-nadir view are used. This solar angle dependence may bring on unreal latitudinal and seasonal dependence of optical thickness in cloud climatology. Hence, the influence of cloud horizontal inhomogeneity should be corrected.

It is suggested that for bias removal some empirical assumptions are required in geometrical and microphysical properties of cloud, which should be studied with in situ observation data. In situ observation is im-

portant for interconnection among geometrical roughness of cloud top, geometrical thickness, and optical thickness. For instance, active sensor such as radar and lidar will provide valuable information of fine-scale structure of cloud-top and in-cloud distribution of liquid water. Furthermore, global observation of cloud inhomogeneity parameter and cloud microphysics with corrections of 3D radiative effects will be the next subject. Statistical quantities of retrieved optical thickness have been investigated in the present study, because parameter estimation of a pixel would be erroneous for moderate-resolution data due to lack of in-pixel information. If very fine-resolution data are available, the reflectance of a small pixel is affected by neighboring pixels rather than in-pixel inhomogeneity. In such a case, a different approach is necessary. A possible method for fine-resolution remote sensing would be a multispectral multipixel method (Marshak et al. 1998; Oreopoulos et al. 2000; Iwabuchi 2000), in which multispectral neighboring pixel data are used to estimate cloud parameters of a pixel.

Acknowledgments. The authors are grateful to Prof. S. Asano of Tohoku University, Japan; Prof. H. Isaka of Universite Blaise Pascal, France; and Dr. K. Kawamoto of NASA Langley Research Center for their helpful comments; and to Dr. N. Kikuchi of Tohoku University, Japan for valuable discussions and providing a basic code of the Monte Carlo model. Thanks are extended to two anonymous reviewers for many good suggestions. Major parts of this work are performed during the course for the first author in the Graduate School of Science, Tohoku University.

APPENDIX

Parameterizations for Bias Removal

It is useful to make some parameterizations available for interpretation of the multiple relationships of ΔM and ΔS^2 on M, S, mean geometrical thickness $\langle Z \rangle$, spectral exponent β, and surface reflectance α_g. Based on the sensitivity studies, the biases ΔM and ΔS^2 can be expressed in the following regression equations:

TABLE A1. Summary of Monte Carlo simulations to determine regression coefficients in Eqs. (A1a) and (A1b).

Parameter	Values	Reference
θ_0	0°, 40°, 60°, 70°	—
S	0.3	0.3
M	0.5, 0.75, 1.0, 1.25, 1.5	1.0
$\langle Z \rangle$ (m)	200, 500, 1000	500
β	1.4, 1.6, 1.8	1.6
α_g	0.0, 0.06, 0.12, 0.2	0.06

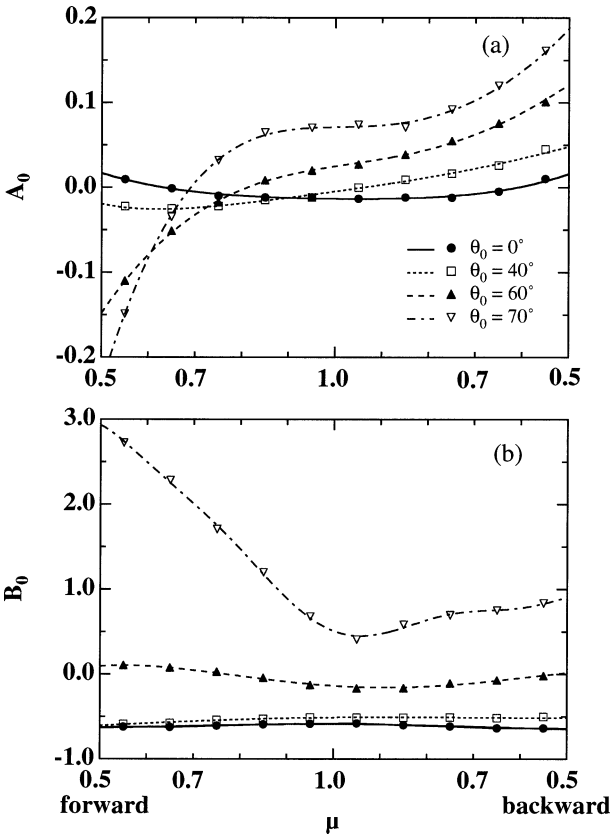

FIG. A1. Viewing angle distributions of regression coefficients (a) A_0 and (b) B_0 in the parameterization formulas for the four solar zenith angles; $\theta_0 = 0°$, 40°, 60°, and 70°.

$$\frac{0.3^2}{S^2}\Delta M = A_0(\mu_0, \mu, \phi) + \sum_{i=1}^{5} A_i(\mu_0, \mu, \phi)X_i + \epsilon_M(\mu_0, \mu, \phi), \tag{A1a}$$

$$\frac{\Delta S^2}{S^2} = B_0(\mu_0, \mu, \phi) + \sum_{i=1}^{5} B_i(\mu_0, \mu, \phi)X_i + \epsilon_{S^2}(\mu_0, \mu, \phi), \tag{A1b}$$

where A_i and B_i are the regression coefficients for each viewing geometry, ϵ_M and ϵ_S^2 are regression errors. The parameters X_I are defined as follows:

$$X_1 \equiv (M - 1.0)/0.5, \tag{A2a}$$

$$X_2 \equiv X_1^2, \tag{A2b}$$

$$X_3 \equiv (\sqrt{\langle Z \rangle} - \sqrt{500})/8.22, \tag{A2c}$$

$$X_4 \equiv (\beta - 1.6)/0.2, \tag{A2d}$$

$$X_5 \equiv (\alpha_g - 0.06)/0.1. \tag{A2e}$$

In Eq. (A1a) ΔM is normalized to the reference case with $S = 0.3$. The term $\Delta S^2/S^2$ in Eq. (A1b) represents relative bias in S^2. Each first term in the right-hand side of Eqs. (A1a) and (A1b) A_0 and B_0, represents a ref-

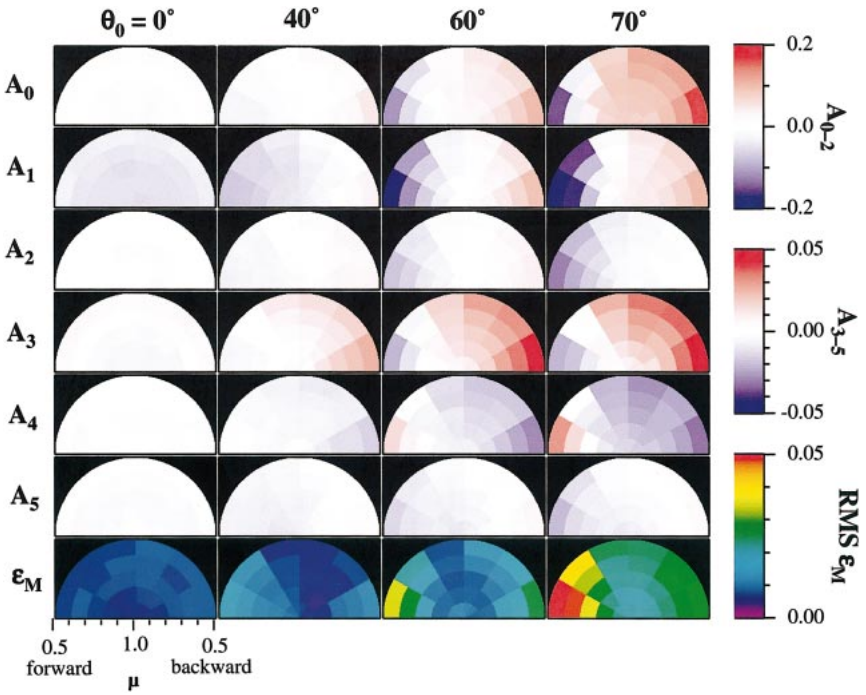

FIG. A2. Polar projections of regression coefficients $A_i (i = 0–5)$ and rms error ε_M in the parameterization formula Eq. (A1a). The radial distance in each plot corresponds to $\mu(>0.5)$, and the azimuth angle from the left-hand direction corresponds to ϕ. The color scaling is different between for $A_{0–2}$ and for $A_{3–5}$.

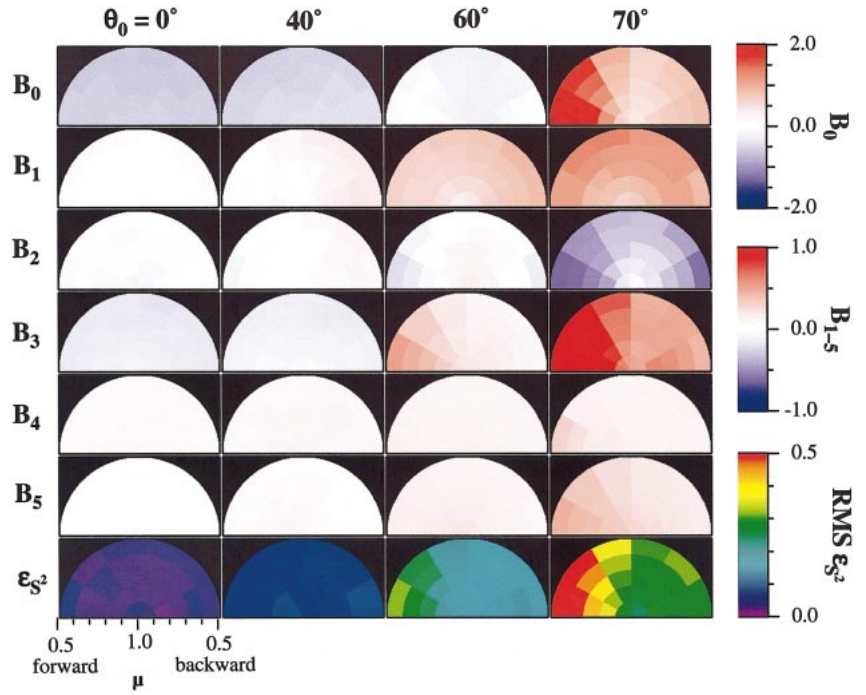

FIG. A3. As in Fig. A2, except for B_i and ε_S^2 in Eq. (A1b). The color scaling is different between for B_0 and for $B_{1–5}$.

erence of the normalized ΔM and the relative ΔS^2, respectively, since the other terms vanish in the reference case with $M = 1$, $\langle Z \rangle = 500$ m, $\beta = 1.6$, and $\alpha_g = 0.06$. The other terms represent the deviations from the reference, and the coefficients A_i, B_i, represent the sensitivities to X_i for $i = 1$–5, respectively. To determine the coefficients A_i and B_i, extensive simulations were carried out for 720 cases. The values of parameters used in the simulations are summarized in Table A1. The RC2 model was used. The coefficients A_i and B_i are computed by the multiple regression analysis for each bidirectional angle independently.

Figure A1 shows the angular distribution of A_0 and B_0 for near-solar plane ($\phi = 0°$–$30°$ in the left-hand side, $\phi = 150°$–$180°$ in the right-hand side). In Fig. A1a, the cloud side effects, that is, shadowing in forward view and illumination in backward view, are clearly shown for A_0 for low solar elevation. For nadir view, A_0 increases with increasing solar zenith angle. This is consistent with observed solar angle dependence of mean AVHRR nadir reflectance (Loeb and Coakley 1998). The value of B_0 (Fig. A1b) markedly differs by the solar zenith angle, especially for large solar zenith angle. For high solar elevation ($\theta_0 < 40°$), it is found that IPA-based retrieved inhomogeneity ($S^2_{\rm ipa}$) will be about half of the true value; the inhomogeneous cloud field looks very smooth. On the other hand, B_0 increases rapidly for $\theta_0 > 60°$, especially in the forward view. In other words, the roughening rapidly increases with increasing solar zenith angle.

Figure A2 shows polar plots of the bidirectional angular distribution of the regression coefficients A_i. The distribution of A_i suggests that the angular dependence of ΔM quantitatively changes by condition. A positive value of A_i means that ΔM increases with increasing X_i and vice versa. A positive correlation of A_1 with A_0 indicates that an increase in M enhances the angular dependence of ΔM. It is also suggested that an increase in $\langle Z \rangle$ enhances the angular dependence of ΔM. Contrarily, a negative correlation of A_4 with A_0 indicates that decrease in β enhances the angular dependence of ΔM. In other words, the effect of horizontal radiative transport on $M_{\rm ipa}$ is enhanced for an optically and geometrically thick cloud with small spectral exponent. The bias ΔM is mainly sensitive to M; that is, the absolute value of A_1 is largest among A_i for $i = 1$–5. The sensitivities of ΔM to $\langle Z \rangle$ and β is about one fourth as large as the sensitivity to M, while α_g does not dominate to determine ΔM. Figure A3 is the same as Fig. A2, except for B_i. It is shown that B_0 changes mainly by the solar zenith angle. The absolute values of coefficients B_1 and B_3 are relatively large, so that M and $\langle Z \rangle$ are important to determine the spatial variability of $\log\tau_{\rm ipa}$ (and of reflected radiation). As compared with them, β and α_g are not dominant for interpreting the spatial variability. A large positive value of B_1 for oblique sun indicates that radiance field looks rough substantially for an optically thick case. A positive correlation of B_3 with B_0 indicates that the angular dependence of ΔS^2 is enhanced for geometrically thick cloud, since horizontal radiative transport increases. A positive value is always kept for B_4, because of the masking effect by finite spatial resolution. The coefficient B_5 is also always positive, so that variance of $\log\tau_{\rm ipa}$ is large for bright underlying surface though the sensitivity is not high. The last rows in the bottom of Figs. A2 and A3 show root-mean-square (rms) errors of the regression formulas Eqs. (A1a) and (A1b). For $\theta_0 = 60°$, the rms error is 0.015 for ϵ_M and 0.18 for ϵ^2_S, on average. The error originates from Monte Carlo noise, realization of cloud by stochastic model, and nonlinearity and multiple colinearity of the regression formulas. The error due to Monte Carlo noise was estimated at 0.005 for ϵ_M on average and 0.089 for ϵ^2_S, when photons of 10^7 were used. These errors are almost the same as those due to stochastic cloud realizations. It is suggested that the regression formulas well represent relationships of the biases to multiparameters though the rms error is relatively large for oblique sun, especially in the forward view.

A set of Eqs. (A1a) and (A1b), and definitions of ΔM and ΔS^2 [(6a) and (6b)] can be easily applied to correct retrieved optical thickness from satellite observation. These equations consist of a nonlinear system of M and S, which are solved from iteration of calculation of ΔM and ΔS^2 and the revision of M and S^2 with bias correction. The true moments, M and S, are estimated from observed ones, $M_{\rm ipa}$ and $S_{\rm ipa}$, if $\langle Z \rangle$, β, and α_g are provided. The mean and standard deviation of optical thickness can be estimated as by-product from M and S, using Eqs. (4) and (5). A main advantage of the parameterizations is that they can be used after conventional IPA retrieval (i.e., no reanalysis is required). Furthermore, these results have some contribution toward the direct problem of cloud inhomogeneity. The domain-averaged reflectance can be calculated by the same procedure as effective thickness approximation (Cahalan et al. 1994b) or the lognormal IPA (Oreopoulos and Davies 1998b), assuming that the frequency distribution of optical thickness obeys lognormal distribution with the mean and standard deviation, $M_{\rm ipa}$ and $S_{\rm ipa}$, respectively.

REFERENCES

Barker, H. W., 1996: Estimating cloud field albedo using one-dimensional series of optical depth. *J. Atmos. Sci.,* **53,** 2826–2836.

——, and J. A. Davies, 1992a: Cumulus cloud radiative properties and the characteristics of satellite radiance wavenumber spectra. *Remote Sens. Environ.,* **42,** 51–64.

——, and ——, 1992b: Solar radiative fluxes for stochastic, scale-invariant broken cloud fields. *J. Atmos. Sci.,* **49,** 1115–1126.

——, and D. Liu, 1995: Inferring optical depth of broken clouds from Landsat data. *J. Climate,* **8,** 2620–2630.

Boers, R., J. D. Spinhirne, and W. D. Hart, 1988: Lidar observations of the fine-scale variability of marine stratocumulus clouds. *J. Appl. Meteor.,* **27,** 797–810.

Bower, K. N., T. W. Choularton, J. Latham, J. Nelson, M. B. Baker, and J. Jensen, 1994: A parameterization of warm clouds for use

in atmospheric general circulation models. *J. Atmos. Sci.,* **51,** 2722–2732.

Cahalan, R. F., W. Ridgway, and W. J. Wiscombe, 1994a: Independent pixel and Monte Carlo estimates of the stratocumulus albedo. *J. Atmos. Sci.,* **51,** 3776–3790.

——, ——, ——, T. L. Bell, and J. B. Snider, 1994b: The albedo of fractal stratocumulus clouds. *J. Atmos. Sci.,* **51,** 2434–2455.

Chambers, L. H., B. A. Wielicki, and K. F. Evans, 1997: Accuracy of the independent pixel approximation for satellite estimates of oceanic boundary layer cloud optical depth. *J. Geophys. Res.,* **102,** 1779–1794.

Davis, A. B., A. Marshak, R. F. Cahalan, and W. J. Wiscombe, 1997: The Landsat scale break in stratocumulus as a three-dimensional radiative transfer effect: Implications for cloud remote sensing. *J. Atmos. Sci.,* **54,** 241–260.

Drake, F., 1993: Global cloud cover and liquid water path from ISCCP C2 data. *Int. J. Climatol.,* **13,** 581–605.

Duda, D. P., G. L. Stephens, B. Stevens, and W. R. Cotton, 1996: Effects of aerosol and horizontal inhomogeneity on the broadband albedo of marine stratus: Numerical simulations. *J. Atmos. Sci.,* **53,** 3757–3769.

Evans, F. K., 1993: Two-dimensional radiative transfer in cloudy atmospheres: The spherical harmonic spatial grid method. *J. Atmos. Sci.,* **50,** 3111–3124.

Hayasaka, T., M. Kuji, and M. Tanaka, 1994: Air truth validation of cloud albedo estimated from NOAA advanced very high resolution radiometer data. *J. Geophys. Res.,* **99,** 18 685–18 693.

——, N. Kikuchi, and M. Tanaka, 1995: Absorption of solar radiation by stratocumulus clouds: Aircraft measurements and theoretical calculations. *J. Appl. Meteor.,* **34,** 1047–1055.

Iwabuchi, H., 2000: Effects of cloud horizontal inhomogeneity on optical remote sensing of cloud parameters. Ph.D. thesis, Tohoku University, Sendai, Japan,104 pp.

Kawamoto, K., T. Nakajima, and T. Y. Nakajima, 2001: A global determination of cloud microphysics AVHRR remote sensing. *J. Climate,* **14,** 2054–2068.

Kikuchi, K., Y. Asuma, T. Taniguchi, M. Kanno, M. Tanaka, T. Hayasaka, T. Takeda, and Y. Fujiyoshi, 1993: Structure and reflectance of winter maritime stratocumulus clouds. *J. Meteor. Soc. Japan,* **71,** 715–731.

Kneizys, F. X., E. P. Shettle, L. W. Abreu, J. H. Chetwynd, G. P. Anderson, W. O. Gallery, J. E. A. Selby, and S. A. Clough, 1988: Users Guide to LOWTRAN 7. Air Force Geophys. Lab. Tech. Rep. AFGL-TR-88-0177, 137 pp.

Kobayashi, T., 1993: Effects due to cloud geometry on biases in the albedo derived from radiance measurements. *J. Climate,* **6,** 120–128.

Loeb, N. G., and J. A. Coakley Jr., 1998: Inference of marine stratus cloud optical depth from satellite measurements: Does 1D theory apply? *J. Climate,* **11,** 215–233.

——, T. Várnai, and D. M. Winker, 1998: Influence of subpixel-scale cloud-top structure on reflectances from overcast stratiform cloud layers. *J. Atmos. Sci.,* **55,** 2960–2973.

Marshak, A., A. Davis, W. J. Wiscombe, and R. F. Cahalan, 1995a: Radiative smoothing in fractal clouds. *J. Geophys. Res.,* **100,** 26 247–26 261.

——, ——, ——, and G. Titov, 1995b: The verisimilitude of the independent pixel approximation used in cloud remote sensing. *Remote Sens. Environ.,* **52,** 71–78.

——, ——, R. F. Cahalan, and W. J. Wiscombe, 1998: Nonlocal independent pixel approximation: Direct and inverse problems. *IEEE Trans. Geosci. Remote Sens.,* **36,** 192–205.

——, ——, W. J. Wiscombe, and R. F. Cahalan, 1999: Horizontal radiative fluxes in clouds and accuracy of the independent pixel approximation at absorbing wavelengths. *Geophys. Res. Lett.,* **26,** 1585–1588.

Minnis, P., P. W. Heck, D. F. Young, C. W. Fairall, and J. B. Snider, 1992: Stratocumulus cloud properties derived from simultaneous satellite and island-based instrumentation during FIRE. *J. Appl. Meteor.,* **31,** 317–339.

Nakajima, T., and M. D. King, 1990: Determination of the optical thickness and effective particle radius of clouds from reflected solar radiation measurements. Part I: Theory. *J. Atmos. Sci.,* **47,** 1878–1893.

Oreopoulos, L., and R. Davies, 1998a: Plane parallel albedo biases from satellite observations. Part I: Dependence on resolution and other factors. *J. Climate,* **11,** 919–932.

——, and ——, 1998b: Plane parallel albedo biases from satellite observations. Part II: Parameterizations for bias removal. *J. Climate,* **11,** 933–944.

——, A. Marshak, R. F. Cahalan, and G. Wen, 2000: Cloud three-dimensional effects evidenced in Landsat spatial power spectra and autocorrelation functions. *J. Geophys. Res.,* **105,** 14 777–14 788.

Pawlowska, H., and Coauthors, 2000: Microphysical and radiative properties of stratocumulus clouds: The EUCREX mission 206 case study. *Atmos. Res.,* **55,** 85–102.

Pincus, R., S. A. McFarlane, and S. A. Klein, 1999: Albedo bias and the horizontal variability of clouds in the subtropical marine boundary layers: Observations from ships and satellites. *J. Geophys. Res.,* **104,** 6183–6191.

Rossow, W. B., and R. A. Schiffer, 1991: ISCCP cloud data products. *Bull. Amer. Meteor. Soc.,* **72,** 2–20.

Szczap, F., H. Isaka, M. Saute, B. Guillemet, and Y. Gour, 2000: Inhomogeneity effects of 1D and 2D bounded cascade model clouds on their effective radiative properties. *Phys. Chem. Earth,* **25,** 83–89.

Titov, G. A., 1998: Radiative horizontal transport and absorption in stratocumulus clouds. *J. Atmos. Soc.,* **55,** 2549–2560.

Tselioudis, G., W. B. Rossow, and D. Rind, 1992: Global patterns of cloud optical thickness variation with temperature. *J. Climate,* **5,** 1484–1495.

Vali, G., R. D. Kelly, J. French, S. Haimov, and D. Leon, 1998: Finescale structure and microphysics of coastal stratus. *J. Atmos. Sci.,* **55,** 3540–3564.

Várnai, T., 2000: Influence of three-dimensional radiative effects on the spatial distribution of shortwave cloud reflection. *J. Atmos. Sci.,* **57,** 216–229.

——, and R. Davies, 1999: Effects of cloud heterogeneities on shortwave radiation: Comparison of cloud-top variability and internal heterogeneity. *J. Atmos. Sci.,* **56,** 4206–4224.

Zuidema, P., and K. F. Evans, 1998: On the validity of the independent pixel approximation for boundary layer cloud observed during ASTEX. *J. Geophys. Res.,* **103,** 6059–6074.